Real-Time Estimation of VPP Equivalent Inertia and Fast Frequency Control

Weilin Zhong, Georgios Tzounas, and Federico Milano
School of Electrical & Electronic Engineering, University College Dublin, Ireland
weilin.zhong@ucdconnect.ie, georgios.tzounas@ucd.ie, federico.milano@ucd.ie

***Abstract*— The paper proposes a method to estimate, in transient conditions, the equivalent inertia constant and fast frequency control droop gain of Virtual Power Plants (VPPs). The estimations are obtained based on the frequency and active power variations at the point of connection of the VPP with the power grid. The accuracy of the estimator is enhanced by a novel technique employed to approximate the VPP's equivalent internal reactance, based on the voltage and reactive power variations at the point of connection. The performance of the proposed method is illustrated through a case study based on a modified version of the WSCC 9-bus system.**

***Index Terms*— Dynamic state estimation, Virtual Power Plant (VPP), equivalent inertia, Fast Frequency Response (FFR).**

I. Introduction

A. Motivation

A Virtual Power Plant (VPP) aggregates the capacities of several devices, e.g. Distributed Energy Resources (DERs), Energy Storage Systems (ESSs) and dispatchable loads, which are controlled to operate like one grid-connected generator [1]. The devices that compose a VPP are typically connected to the grid through power converters and thus, in contrast to Synchronous Machines (SMs), they do not provide mechanical inertia to the system. However, these devices can be designed to emulate the inertial response of SMs, as well as to regulate the frequency, thus enhancing the system's overall stability and performance. How to estimate on-line and accurately the equivalent inertia and the equivalent Fast Frequency Response (FFR) of a VPP is the topic discussed in this paper.

B. Literature Review

The rotational inertia of SMs plays a crucial role in maintaining the frequency during the first instants that follow the occurrence of a contingency or of a large power imbalance in the network. However, this inertia is reducing as a result of the gradual substitution of SMs by non-synchronous devices. In general, systems with lower inertia show larger frequency and Rate of Change of Frequency (RoCoF) variations and hence are more prone to instability and blackouts [2]. Hence, during the last decade there has been a growing interest on the stability and control of low-inertia systems as well as on establishing methods to estimate the system's inertia in a precise and fast way [3]–[5]. If properly controlled, non-synchronous devices can provide inertial response and frequency regulation services that are similar to the ones provided by SMs. Recent studies propose control schemes that tackle this problem, with some of them focusing on the coordination of devices that comprise VPPs, see [1], [6]–[9].

The inertial response of non-synchronous devices is a result of a control and is not generally based on an actual rotational inertia. It is thus relevant to evaluate how this control compares with rotational inertia. In this vein, [10] presents a formula to estimate, in transient conditions, the equivalent inertia of both synchronous and non-synchronous devices. Based on [10], the authors in [11] propose an inertia estimator with improved numerical stability and provide, as a byproduct, a formula to track the FFR droop gain of non-synchronous devices.

The estimators presented in [10] and [11] track the inertia of a single device connected to a bus of the network and under the assumption that the device's internal reactance is known. However, a VPP typically consists of many resources that are dispersed in multiple buses of the network and thus, defining the total equivalent reactance of a VPP is not straightforward. In this vein, a technique to estimate the equivalent internal reactance and then the inertia of a VPP is proposed in [12]. The method in [12] imposes for the estimation a simplified SM model without damping which does not allow an estimation of the equivalent FFR droop gain of the VPP.

C. Contributions

The paper presents a method to track in real-time the equivalent inertia of a VPP. The estimator relies on a novel approach to determine the VPP's internal equivalent reactance. The SM model imposed to the VPP for the estimation takes into account the machine's damping, which first, leads to improved accuracy of the estimation and second, allows estimating the VPP's equivalent FFR droop gain. The accuracy of the proposed approach is first validated for synchronous, and then applied to non-synchronous devices, as well as to a VPP comprising multiple DERs, loads, and an ESS.

D. Organization

The remainder of the paper is organized as follows. Section II briefly provides the theoretical background behind our approach to inertia estimation in this paper. Section III reviews the inertia estimation method developed in [11] and extends it to formulate the proposed equivalent inertia and FFR droop gain estimation for VPPs. Section IV presents a case study based on the WSCC 9-bus system. Finally, conclusions and future work directions are discussed in Section V.

This work was supported by Science Foundation Ireland, by funding W. Zhong and F. Milano under project ESIPP, grant no. SFI/15/SPP/E3125; and by the European Commission, by funding G. Tzounas and F. Milano under the project EdgeFLEX, grant agreement no. 883710.

II. Background

We provide a theoretical background starting from the well-known power flow equations. The concepts described in this section are utilized in Section III-B for the estimation of the VPP equivalent inertia and FFR droop gain. Let us consider first the complex power injections at a network with n buses, namely $\bar{\boldsymbol{s}} \in \mathbb{C}^{n\times 1}$, as follows:

$$\bar{\boldsymbol{s}}(t) = \boldsymbol{p}(t) + j\boldsymbol{q}(t) = \bar{\boldsymbol{v}}(t) \circ \left(\bar{\mathbf{Y}}\,\bar{\boldsymbol{v}}(t)\right)^{*}, \tag{1}$$

where $\boldsymbol{p}, \boldsymbol{q} \in \mathbb{C}^{n\times 1}$ are the bus active and reactive power injections, respectively; $\bar{\boldsymbol{v}} \in \mathbb{C}^{n\times 1}$ is the vector of the bus voltages; $\bar{\mathbf{Y}} \in \mathbb{C}^{n\times n}$ is the admittance matrix of the network; $\circ$ denotes the element-wise multiplication; and $*$ represents the conjugate of a complex quantity.

Let us rewrite (1) using an element-wise notation:

$$\begin{aligned} p_h &= \sum_{k=1}^{n} v_h v_k \left(G_{h,k}\cos\theta_{h,k} + B_{h,k}\sin\theta_{h,k}\right), \\ q_h &= \sum_{k=1}^{n} v_h v_k \left(G_{h,k}\sin\theta_{h,k} - B_{h,k}\cos\theta_{h,k}\right), \end{aligned} \tag{2}$$

where the dependency on time has been dropped for simplicity; p_h, q_h are the h-th elements of $\boldsymbol{p}$, $\boldsymbol{q}$; $G_{h,k}$, $B_{h,k}$ are the real and imaginary parts of the (h,k) element of $\bar{\mathbf{Y}}$, i.e. $\bar{Y}_{h,k} = G_{h,k} + jB_{h,k}$; v_k is the voltage magnitude at bus k; and $\theta_{h,k} = \theta_h - \theta_k$, where θ_h and θ_k are the voltage phase angles at buses h and k, respectively. We differentiate (2) and rewrite the deviation of the active and reactive power injections at bus h as the sum of two components [13]:

$$dp_h = \sum_{k=1}^{n} \frac{\partial p_h}{\partial \theta_{h,k}} d\theta_{h,k} + \sum_{k=1}^{n} \frac{\partial p_h}{\partial v_k} dv_k \equiv dp'_h + dp''_h, \tag{3}$$

$$dq_h = \sum_{k=1}^{n} \frac{\partial q_h}{\partial \theta_{h,k}} d\theta_{h,k} + \sum_{k=1}^{n} \frac{\partial q_h}{\partial v_k} dv_k \equiv dq'_h + dq''_h, \tag{4}$$

where dp'_h, dq'_h are the quotas of the active and reactive power that depend on the bus voltage phase angle variations, and dp''_h, dq''_h are the corresponding quotas that depend on the bus voltage magnitude variations.

Based on the *complex frequency* concept presented in [13], and using a matrix form, the quotas dp'_h, dq''_h (denoted in matrix form as $\dot{\boldsymbol{p}}'$, $\dot{\boldsymbol{q}}''$) can be approximately expressed as:

$$\dot{\boldsymbol{p}}' \approx \boldsymbol{B}'\boldsymbol{\omega}, \tag{5}$$

$$\dot{\boldsymbol{q}}'' \approx \boldsymbol{B}''\boldsymbol{\varrho}, \tag{6}$$

where $B'_{h,k} = -B_{h,k}$, $B'_{h,h} = \sum_{h\neq k}^{n} B_{h,k}$ are the elements of $\boldsymbol{B}'$ and $B''_{h,k} = -B_{h,k}$, $B''_{h,h} = -2B_{h,h}$ are the elements of $\boldsymbol{B}''$; $\boldsymbol{\omega}$ is the vector of bus frequencies; and the vector $\boldsymbol{\varrho} \equiv \dot{\boldsymbol{v}}/\boldsymbol{v}$ represents the transient rate of change of the bus voltages normalized with respect to their magnitude.

Equations (5) and (6) exploit the fact that dp'_h is the component of the active power that can effectively modify the frequency in the grid, whereas the impact of dp''_h on the frequency is negligible. Similarly, dq''_h is the component of the reactive power that varies the most when the voltage at bus h is regulated, whereas the contribution of dq'_h to the voltage regulation is negligible. Equations (5) and (6) are duly utilized in the next section for the inertia and FFR droop gain estimation of VPPs.

III. Inertia and FFR Gain Estimation

In this section, we first recall the method developed in [11] for the inertia estimation of a single device connected to a bus of a power network, and then describe the proposed equivalent inertia and FFR droop gain estimator for VPPs.

A. Inertia Estimation of Synchronous Machines

The effect of the inertia constant M_{G} of a SM on its dynamics is described through the swing equation:

$$M_{\mathrm{G}}\dot{\omega}_{\mathrm{G}} = p_{\mathrm{m}} - p_{\mathrm{G}} - D_{\mathrm{G}}(\omega_{\mathrm{G}} - \omega_o), \tag{7}$$

where ω_o is the SM's rated rotor speed; ω_{G} is the SM's rotor speed and $\dot{\omega}_{\mathrm{G}}$ its time derivative; p_{m} is the mechanical power provided by the turbine; p_{G} is the electrical power that the SM injects to the grid; and D_{G} is the damping coefficient.

We decompose p_{m} into the following three terms:

$$p_{\mathrm{m}} = p_{\mathrm{PFC}} + p_{\mathrm{SFC}} + p_{\mathrm{UC}}, \tag{8}$$

where p_{PFC} is the active power regulated by the Primary Frequency Control (PFC); p_{SFC} is the active power regulated by the Secondary Frequency Control (SFC); and p_{UC} is the power set point determined by solving the Unit Commitment (UC) problem. The PFC and SFC for a SM are typically achieved through the Turbine Governor (TG) and Automatic Generation Control (AGC), respectively.

Merging (7) and (8) and differentiating with respect to time:

$$M_{\mathrm{G}}\ddot{\omega}_{\mathrm{G}} = \dot{p}_{\mathrm{PFC}} + \dot{p}_{\mathrm{SFC}} + \dot{p}_{\mathrm{UC}} - \dot{p}_{\mathrm{G}} - D_{\mathrm{G}}\dot{\omega}_{\mathrm{G}}. \tag{9}$$

Considering the time scale of inertial response of the SM, in the very first instants after a contingency, one can assume that $\dot{p}_{\mathrm{UC}} \approx 0$, $\dot{p}_{\mathrm{SFC}} \approx 0$, and $|\dot{p}_{\mathrm{PFC}}| \ll |\dot{p}_{\mathrm{G}}|$. Then, one has:

$$M_{\mathrm{G}} \approx -\frac{\dot{p}_{\mathrm{G}} + D_{\mathrm{G}}\dot{\omega}_{\mathrm{G}}}{\ddot{\omega}_{\mathrm{G}}}. \tag{10}$$

Note that when $\ddot{\omega}_{\mathrm{G}}$ crosses zero following a contingency, a singularity occurs in (10). This singularity can be avoided if, instead of (10), the following equation is used to compute M_{G}:

$$T_M\dot{M}_{\mathrm{G}} = \gamma(\ddot{\omega}_{\mathrm{G}})\left(\dot{p}_{\mathrm{G}} + M_{\mathrm{G}}\ddot{\omega}_{\mathrm{G}} + D_{\mathrm{G}}\dot{\omega}_{\mathrm{G}}\right), \tag{11}$$

while the following equation allows estimating D_{G} [11]:

$$T_D\dot{D}_{\mathrm{G}} = \gamma(\Delta\omega_{\mathrm{G}})\left(\Delta p_{\mathrm{G}} + M_{\mathrm{G}}\dot{\omega}_{\mathrm{G}} + D_{\mathrm{G}}\Delta\omega_{\mathrm{G}}\right), \tag{12}$$

where

$$\Delta\omega_{\mathrm{G}} = \int \dot{\omega}_{\mathrm{G}} dt, \qquad \Delta p_{\mathrm{G}} = \int \dot{p}_{\mathrm{G}} dt, \tag{13}$$

and $\gamma(y)$ is defined as:

$$\gamma(y) = \begin{cases} -1, & y \geq \epsilon_y, \\ 0, & -\epsilon_y < y < \epsilon_y, \\ 1, & y \leq -\epsilon_y, \end{cases} \tag{14}$$

where ϵ_y is a small positive threshold that helps reduce the impact of noise and improve the accuracy of $\gamma(y)$. A good choice for ϵ_y is in the range $[10^{-7}, 10^{-5}]$.

The term $\dot{p}_{\rm G} + M_{\rm G}\ddot{\omega}_{\rm G} + D_{\rm G}\dot{\omega}_{\rm G}$ is zero at the equilibrium and non-zero during transients. Consider an example for which $\dot{p}_{\rm G} + M_{\rm G}\ddot{\omega}_{\rm G} + D_{\rm G}\dot{\omega}_{\rm G} > 0$. The sign of $\ddot{\omega}_{\rm G}$ decides the sign of $\gamma(\ddot{\omega}_{\rm G})$. If $\ddot{\omega}_{\rm G} > 0$, $M_{\rm G}$ has to decrease, to also reduce $\dot{p}_{\rm G} + M_{\rm G}\ddot{\omega}_{\rm G} + D_{\rm G}\dot{\omega}_{\rm G}$ and converge to the equilibrium. In this case, $\dot{M}_{\rm G} < 0$ and thus $\gamma(\ddot{\omega}_{\rm G}) = -1$. Vice versa, if $\ddot{\omega}_{\rm G} < 0$, $M_{\rm G}$ has to increase and thus $\gamma(\ddot{\omega}_{\rm G}) = 1$. The rate of change of $M_{\rm G}$ is defined by the time constant T_M. A small T_M tracks $M_{\rm G}$ faster, although it might generate numerical oscillations. Hence, we consider T_M, T_D in the time scale of the inertial response, i.e. $T_M, T_D \in [10^{-3}, 10^{-2}]$ s. The rationale behind (12) can be described in a similar way.

B. Proposed VPP Inertia Estimation

The expressions (11) and (12) can be extended to any non-synchronous device that is controlled to provide a similar dynamic response with a SM in the inertial response time scale. For a non-synchronous device, one has [11]:

$$\begin{aligned} T_M \dot{M}_{{\rm D},h} &= \gamma\big(\ddot{\omega}_{{\rm D},h}\big)\big(\dot{p}'_h + M_{{\rm D},h}\ddot{\omega}_{{\rm D},h} + D_{{\rm D},h}\dot{\omega}_{{\rm D},h}\big)\,, \\ T_D \dot{D}_{{\rm D},h} &= \gamma\big(\Delta\omega_{{\rm D},h}\big)\big(\Delta p'_h + M_{{\rm D},h}\dot{\omega}_{{\rm D},h} + D_{{\rm D},h}\Delta\omega_{{\rm D},h}\big)\,, \end{aligned} \tag{15}$$

where the index ${}_{{\rm D},h}$ represents the device connected to bus h; and $\dot{p}'_h$ is the derivative of the quota of the active power that varies the frequency at bus h (see also Section II). The presence of $D_{{\rm D},h}$ in (15) can enhance the accuracy of the estimator while being meaningful, since it can be understood as the equivalent droop gain of the FFR that the device provides [11]. The internal frequency of the device $\omega_{{\rm D},h}$ is obtained based on (5):

$$\omega_{{\rm D},h} = \Delta\omega_h - x_{{\rm D},h}\dot{p}'_h\,, \tag{16}$$

where $\Delta\omega_h$ is the frequency deviation at bus h; and $x_{{\rm D},h}$ is the equivalent internal reactance of the device.

A poor choice of $x_{{\rm D},h}$ in (16) can significantly affect the accuracy of (15). Most importantly, how to define the equivalent reactance of a VPP is not straightforward, since VPPs aggregate several resources that span multiple buses and thus they may have significant complexity and granularity. In the remainder of this section, we describe a technique to estimate $x_{{\rm D},h}$ based on the voltage and reactive power variations at the point of connection with the rest of the grid [12]. Applying (6) to bus h, we have:

$$\dot{q}''_h \approx B''_h \varrho_h + \sum_{k=1}^{n} B''_{h,k}\varrho_k\,, \tag{17}$$

where ϱ_h, is the h-th element of $\boldsymbol{\varrho}$. In this paper, a low-pass filter is applied to ϱ_h to reduce the reactive power fluctuations and noise. B''_h can be obtained from:

$$B''_h = B''_{{\rm D},h} + B''_{h,h} + \sum_{k=1}^{n} B''_{h,k}\,, \tag{18}$$

where $B''_{{\rm D},h}$ is the equivalent internal susceptance of the device at bus h. From (17), (18), one has:

$$B''_{{\rm D},h} = \frac{\dot{q}''_h - \sum_{k=1}^{n} B''_{h,k}\varrho_k}{\varrho_h} - \sum_{k=1}^{n} B''_{h,k} - B''_{h,h}\,. \tag{19}$$

The equivalent reactance $x_{{\rm D},h}$ can be obtained from the reciprocal of $B_{{\rm D},h}$, as follows:

$$x_{{\rm D},h} = \frac{\varrho_h}{\alpha}\,, \tag{20}$$

where

$$\alpha = \dot{q}''_h - \sum_{k=1}^{n} B''_{h,k}\varrho_k - \left(\sum_{k=1}^{n} B''_{h,k} + B''_{h,h}\right)\varrho_h\,. \tag{21}$$

Equation (20) suffers from the same numerical issue as (10). To overcome the problem, we determine $x_{{\rm D},h}$ using the following differential equation:

$$T_x \dot{x}_{{\rm D},h} = \gamma\big(\alpha\big)\big(x_{{\rm D},h}\alpha - \varrho_h\big)\,, \tag{22}$$

where $\gamma(\alpha)$ is defined by (14), and $T_x \in [10^{-2}, 10^{-1}]$ s.

The equivalent inertia $M_{{\rm D},h}$, FFR droop gain $D_{{\rm D},h}$ and the equivalent reactance $x_{{\rm D},h}$, of the VPP, can finally be estimated through the set of equations (14)-(16) and (21)-(22).

IV. Case Study

In this section, we evaluate the performance of the proposed real-time inertia and FFR droop gain estimation technique, through simulations conducted on the well-known WSCC 9-bus system [14]. The accuracy of the estimator is first checked for SMs, and then applied to a DER and a VPP.

For all scenarios, SMs are modeled with a 4-th order (two-axis) model and are equipped with primary frequency and voltage regulation. A Static Var Compensator (SVC) is also installed at bus 8 of the system. Each load is represented by a Voltage-Dependent Load (VDL) model, where the active and reactive power consumption at the load bus h, say $p_{L,h}$, $q_{L,h}$, are expressed as follows [15]:

$$\begin{aligned} p_{L,h} &= p_{L,h,o}\,(v_h/v_o)^{\alpha_p}\,, \\ q_{L,h} &= q_{L,h,o}\,(v_h/v_o)^{\alpha_q}\,, \end{aligned} \tag{23}$$

where $p_{L,h,o}$, $q_{L,h,o}$ are the rated active and reactive power consumption at bus h; v_h, v_o are the measured and rated voltage at the load bus, respectively; α_p, α_q are the voltage exponents of the active and reactive power, respectively.

All results are obtained with the power system analysis software tool Dome [16] using the following parameters: $\alpha_p = \alpha_q = 1.5$, $T_M = 0.004$ s, $T_D = 0.001$ s, and $T_x = 0.01$ s.

A. Synchronous Machines

We validate the performance of the proposed estimator for the devices that provide mechanical inertia, i.e. SMs. In particular, we focus on the SM connected to bus 2 of the system (denoted as G2). The actual mechanical starting time and damping of G2 are $M_{\rm G2} = 12.8$ s and $D_{\rm G2} = 2.0$, respectively. We assume a 20% increase of the load connected to bus 6 at $t = 1$ s. Figure 1a shows how the proposed estimator compares to the estimator presented in [12]. We note that [12] adopts a simplified expression of (15), as follows:

$$T_M \dot{M}_{{\rm D},h} = \gamma\big(\ddot{\omega}_{{\rm D},h}\big)\big(\dot{p}'_h + M_{{\rm D},h}\ddot{\omega}_{{\rm D},h}\big)\,. \tag{24}$$

The result indicates that including the damping in the SM model imposed for the estimation leads to more accurate

results. Note that the estimator is initialized to zero, and thus it requires 1-2 s of training period to approach the actual inertia and damping values. Moreover, the damping estimation requires more training time than the inertia, since $\Delta\omega_{\mathrm{G}}$ varies more slowly than $\ddot{\omega}_{\mathrm{G}}$ in the first instants after the contingency (see (11), (12)). In the plots, the training period of the estimator is shaded. The values of the estimated quantities in the shaded regions have no physical meaning and should be discarded.

Figure 1b shows that, if the SMs of the system are assumed not to have TGs, the estimator closely tracks the damping coefficient of G2. If TGs are included, the estimator captures the combined effect of the SM's damping plus the droop gain of the PFC. Note that lower TG droop constants R_{TG} lead to higher slopes in the estimated value.

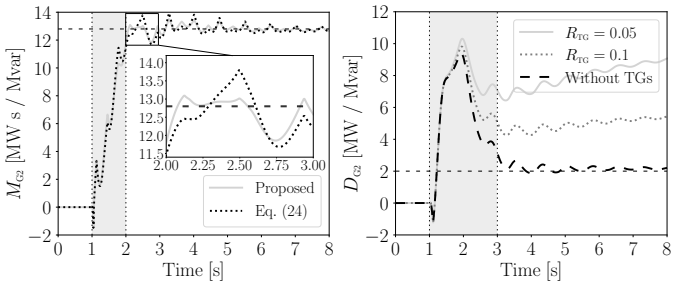

(a) Estimated inertia for G2. (b) Estimated damping for G2.

Fig. 1: 20% increase of load connected to bus 6 at $t = 1$ s.

We study the performance of the proposed estimator when employed for multiple SMs. With this scope, we substitute G2 with a subnetwork (denoted as $\mathrm{D}, 2$) that consists of two SMs and a VDL. The two SMs have in total $M_{\mathrm{D},2} = 18.82$ s, $D_{\mathrm{D},2} = 4.0$, while the rated power consumption of the VDL is $p_{L,2,o} = 0.3$, $q_{L,2,o} = 0.1$ pu. We assume a 20% increase of the load at bus 8 at $t = 1$ s. The estimated inertia and damping of the subnetwork are shown in Fig. 2. As expected, the estimator can accurately track both the inertia and damping of the SMs. Moreover, as expected, inclusion of the PFC impacts more on the damping than on the inertia estimation.

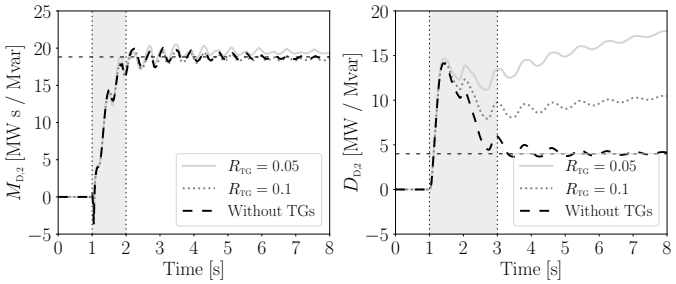

(a) Estimated inertia of $\mathrm{D}, 2$. (b) Estimated Damping of $\mathrm{D}, 2$.

Fig. 2: 20% increase of load connected to bus 8 at $t = 1$ s.

B. Non-Synchronous Devices and VPP

We evaluate the accuracy of the proposed estimator when applied to non-synchronous devices. To this aim, we connect to bus 6 of the WSCC 9-bus system a 45 MW DER (denoted as $\mathrm{D}, 6$), which has the ability to provide frequency control. The DER frequency control is implemented as the parallel of a droop and a RoCoF control channel. We consider at $t = 1$ s a 20% increase of the load at bus 8. Figure 3 shows the estimated trajectories of the equivalent inertia and FFR gain of the DER, as obtained with and without the frequency control (denoted as $\mathrm{FC}_{\mathrm{DER}}$). When $\mathrm{FC}_{\mathrm{DER}}$ is off, we obtain that $M_{\mathrm{D},6} \approx 0$ s and $D_{\mathrm{D},6} \approx 0$, which is as expected. When the DER frequency control is active, we see that both the estimated equivalent inertia and FFR droop gain are time-varying.

A relevant remark is that, in practice, the precision of the estimation is impacted by how much the frequency and active power vary in the time scale of interest. That is, faster and oscillatory variations of $\dot{p}'_h$ and ω_h lead to higher accuracy, whereas slower and smoother variations lead to lower accuracy in the estimation.

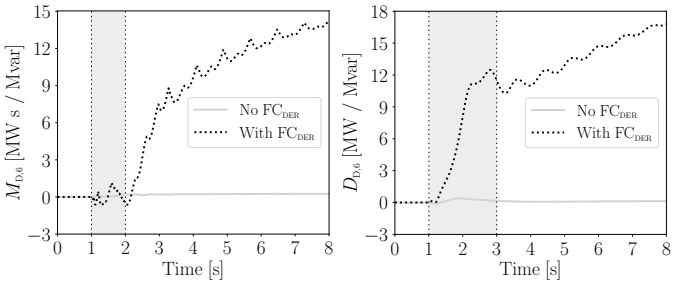

(a) Estimated DER inertia. (b) Estimated DER FFR droop gain.

Fig. 3: 20% increase of load connected to bus 8 at $t = 1$ s.

We finally discuss the suitability of the proposed estimator for evaluating the equivalent inertia and the FFR provided by a VPP. With this scope, the load at bus 6 is substituted by a VPP. The VPP consists of DERs and an ESS, which generate in total 45 MW, and of VDLs with a total power consumption of 57.8 MW. The modified test system is depicted in Fig. 4. The parameters of the VPP are detailed in [17].

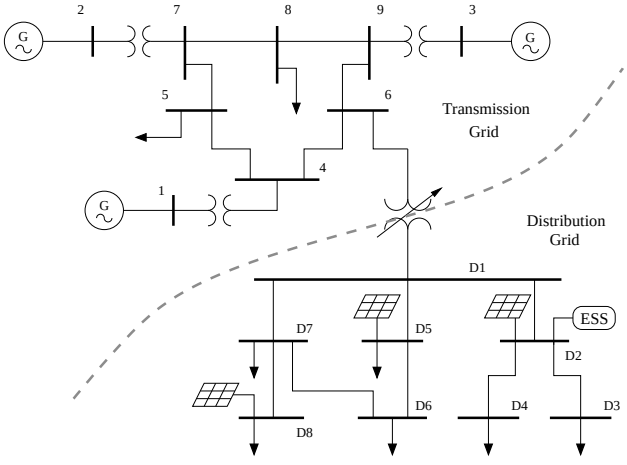

Fig. 4: WSCC 9-bus system modified to include the VPP.

We decrease by 20% the load at bus 5 at $t = 1$ s. Four scenarios within the VPP are evaluated, (i) without ESS nor frequency control provided by the DERs; (ii) without ESS

but with DER frequency control ($\mathrm{FC_{DER}}$); (iii) with ESS but without $\mathrm{FC_{DER}}$; and (iv) with both ESS and $\mathrm{FC_{DER}}$.

The estimated VPP equivalent inertia, FFR gain, as well as the frequency at bus 6 following the disturbance, are depicted in Fig. 5. Results indicate that the VPP provides a time-varying inertia and FFR to the system. The VPP without the ESS nor $\mathrm{FC_{VPP}}$ does not provide any inertia and FFR support to the system, which is consistent with the discussion of Fig. 3 provided above. Moreover, the VPP with ESS and $\mathrm{FC_{DER}}$ can significantly enhance the frequency response of the VPP (see Fig. 5c). Note that in the scenario that the VPP only utilizes the ESS for frequency regulation, it provides only a small equivalent inertia to the system (see Fig. 5a). This is because the ESS reaches quickly its maximum power output and, thereon, it loses its capability to regulate the frequency.

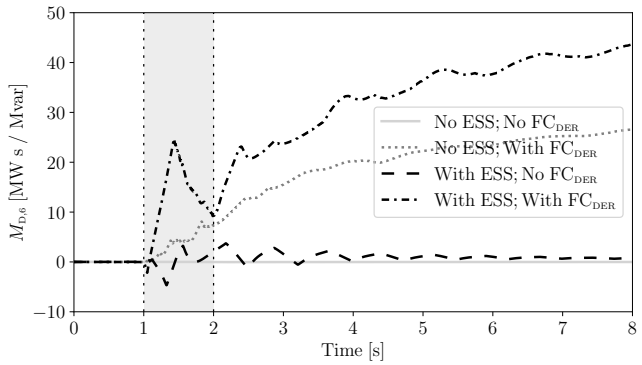

(a) Estimated inertia of VPP.

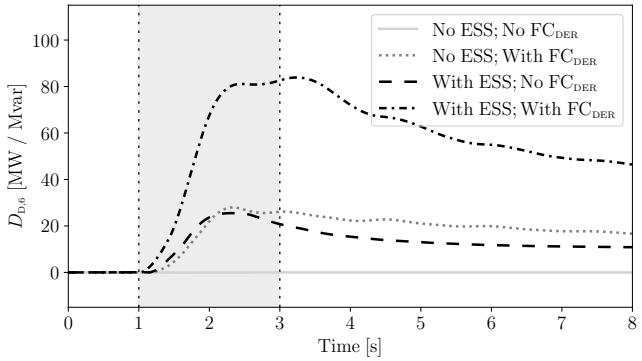

(b) Estimated FFR droop gain of VPP.

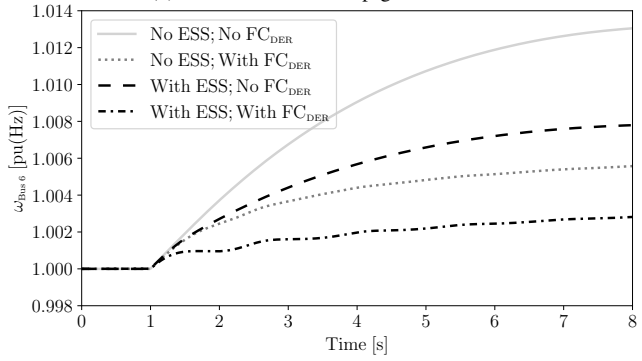

(c) Frequency at bus 6.

Fig. 5: 20% decrease of load connected to bus 5 at $t = 1$ s.

V. Conclusions

This paper proposes a method to estimate the equivalent inertia and FFR droop gain of a VPP. The method includes two steps. First, an estimation of the VPP's internal equivalent reactance is obtained, based on the voltage and power variations at the point of connection of the VPP with the grid. Then, the VPP's equivalent inertia is estimated, by considering for the estimation a classical synchronous machine model with inclusion of damping. The presence of damping in the estimator allows enhancing the accuracy of the estimation, while it provides, as a byproduct, an estimation of the VPP's equivalent FFR droop gain. Simulation results support the proposed estimator by validating its accuracy and suitability for VPP applications.

Future work will focus on exploring applications of the proposed method, including the use of the estimated inertia to improve the dynamic response and efficiency of VPPs.

References

[1] D. Pudjianto, C. Ramsay, and G. Strbac, "Virtual power plant and system integration of distributed energy resources," *IET Renewable power generation*, vol. 1, no. 1, pp. 10–16, 2007.

[2] F. Milano, F. Dörfler, G. Hug, D. J. Hill, and G. Verbič, "Foundations and challenges of low-inertia systems," in *Power Systems Computation Conference (PSCC)*. Dublin, Ireland, 2018, pp. 1–25.

[3] T. Inoue, H. Taniguchi, Y. Ikeguchi, and K. Yoshida, "Estimation of power system inertia constant and capacity of spinning-reserve support generators using measured frequency transients," *IEEE Transactions on Power Systems*, vol. 12, no. 1, pp. 136–143, 1997.

[4] P. M. Ashton, C. S. Saunders, G. A. Taylor, A. M. Carter, and M. E. Bradley, "Inertia estimation of the GB power system using synchrophasor measurements," *IEEE Transactions on Power Systems*, vol. 30, no. 2, pp. 701–709, 2014.

[5] P. Wall and V. Terzija, "Simultaneous estimation of the time of disturbance and inertia in power systems," *IEEE Transactions on Power Delivery*, vol. 29, no. 4, pp. 2018–2031, 2014.

[6] W. Zhong, J. Chen, M. Liu, M. A. A. Murad, and F. Milano, "Coordinated control of virtual power plants to improve power system short-term dynamics," *Energies*, vol. 14, no. 4, p. 1182, 2021.

[7] K. De Brabandere, B. Bolsens, J. Van den Keybus, A. Woyte, J. Driesen, and R. Belmans, "A voltage and frequency droop control method for parallel inverters," *IEEE Transactions on power electronics*, vol. 22, no. 4, pp. 1107–1115, 2007.

[8] R. Majumder, B. Chaudhuri, A. Ghosh, R. Majumder, G. Ledwich, and F. Zare, "Improvement of stability and load sharing in an autonomous microgrid using supplementary droop control loop," *IEEE transactions on power systems*, vol. 25, no. 2, pp. 796–808, 2009.

[9] E. Mashhour and S. M. Moghaddas-Tafreshi, "Bidding strategy of virtual power plant for participating in energy and spinning reserve markets – Part I: Problem formulation," *IEEE Transactions on Power Systems*, vol. 26, no. 2, pp. 949–956, 2010.

[10] F. Milano and Á. Ortega, "A method for evaluating frequency regulation in an electrical grid – Part I: Theory," *IEEE Transactions on Power Systems*, vol. 36, no. 1, pp. 183–193, 2020.

[11] M. Liu, J. Chen, and F. Milano, "On-line inertia estimation for synchronous and non-synchronous devices," *IEEE Transactions on Power Systems*, vol. 36, no. 3, pp. 2693–2701, 2021.

[12] W. Zhong, G. Tzounas, M. Liu, and F. Milano, "On-line inertia estimation of virtual power plants," *Electric Power Systems Research*, 2021, under review. Available online at: faraday1.ucd.ie/vppinert.pdf.

[13] F. Milano, "Complex frequency," *IEEE Transactions on Power Systems*, pp. 1–1, 2021.

[14] P. W. Sauer and M. A. Pai, *Power System Dynamics and Stability*. Prentice hall Upper Saddle River, NJ, 1998, vol. 101.

[15] F. Milano, *Power System Modelling and Scripting*. London: Springer, 2010.

[16] ——, "A Python-based software tool for power system analysis," in *Proceedings of the IEEE PES General Meeting*, Jul. 2013, pp. 1–5.

[17] W. Zhong, M. A. A. Murad, M. Liu, and F. Milano, "Impact of virtual power plants on power system short-term transient response," *Electric Power Systems Research*, vol. 189, p. 106609, 2020.